chemistry

MDPI

Article

Insight into the Adsorption Behavior of Carbon Nanoparticles Derived from Coffee Skin Waste for Remediating Water Contaminated with Pharmaceutical Ingredients

Mutaz Salih [1], Babiker Y. Abdulkhair [2,*] and Mansour Alotaibi [3]

[1] Hurrymilla Applied College, Imam Mohammad Ibn Saud Islamic University (IMSIU), P.O. Box 5701, Riyadh 11432, Saudi Arabia; meamin@imamu.edu.sa
[2] Chemistry Department, College of Science, Imam Mohammad Ibn Saud Islamic University (IMSIU), P.O. Box 90905, Riyadh 11623, Saudi Arabia
[3] Institute of Refining and Petrochemical Technology, KACST, Riyadh 11442, Saudi Arabia; msalotaybi@kacst.edu.sa
* Correspondence: byabdulkhair@imamu.edu.sa or babiker35.by@gmail.com

Abstract: Coffee skins, a cheap, agricultural waste, were carbonized in a tubular furnace under a nitrogen stream and then ball milled to fabricate coffee skin-carbon-nanoparticles (CCNPs). SEM showed 35.6–41.6 nm particle size. The 26.64 and 43.16 peaks in the XRD indicated a cubic graphite lattice. The FT-IR broadband revealed a 2500–3500 cm^{-1} peak, suggesting an acidic O-H group. CCNPs possessed a type-H3-loop in the N_2-adsorption-desorption analysis, with a surface of 105.638 m^2 g^{-1}. Thereafter, CCNPs were tested for ciprofloxacin (CPXN) adsorption, which reached equilibrium in 90 min. CCNPs captured 142.6 mg g^{-1} from 100 mg L^{-1} CPXN, and the 5:12 sorbent mass-to-solution volume ratio was suitable for treating up to 75 mg L^{-1} contamination. The q_t dropped from 142.6 to 114.3 and 79.2 mg g^{-1} as the temperature rose from 20 °C to 35 °C and 50 °C, respectively, indicating exothermic adsorption. CPXN removal efficiency decreased below pH 5.0 and above pH 8.0. Kinetically, CPXN adsorption fits the second-order model and is controlled by the liquid-film mechanism, indicating its preference for the CCNPs' surface. The adsorption agreement with the liquid-film and Freundlich models implied the ease of CPXN penetration into the CCNP inner shells and the multilayered accumulation of CPXN on the CCNPs' surface. The negative ΔH° and ΔG° revealed the exothermic nature and spontaneity of CPXN adsorption onto the CCNP. The CCNPs showed an efficiency of 95.8% during four consecutive regeneration-reuse cycles with a relative standard deviation (RSD) of 3.1%, and the lowest efficiency in the fourth cycle was 92.8%.

Keywords: agriculture waste; coffee skin; carbon nanoparticles; ball milling; water treatment; pharmaceutical pollutant

Citation: Salih, M.; Abdulkhair, B.Y.; Alotaibi, M. Insight into the Adsorption Behavior of Carbon Nanoparticles Derived from Coffee Skin Waste for Remediating Water Contaminated with Pharmaceutical Ingredients. *Chemistry* **2023**, *5*, 1870–1881. https://doi.org/10.3390/chemistry5030128

Academic Editor: Michela Alfè

Received: 20 July 2023
Revised: 21 August 2023
Accepted: 22 August 2023
Published: 24 August 2023

1. Introduction

The importance of water to human survival cannot be overstated because of its essential role in human survival. Pharmaceutical contaminants (PhCs) have been found to accumulate in water and wastewater systems due to their high demand and widespread use [1,2]. Such unpurified water has affected the welfare of people through waterborne diseases that have destroyed the population of cities worldwide [3]. About 80% of marine environmental contaminants originate on land, directly from industrial processes or indirectly through the disposal of diverse residues from human activities [4]. The primary sources of contaminating aquatic environments are industrial cleaning equipment, pesticide runoff from farms, excretions of humans and livestock, dumping of industrial wastes and improper disposal of expired products; these chemicals stay stable in water for a long time [5]. According to the United Nations (UN), over 80% of the world's wastewater is discarded untreated into the environment; in certain countries, the percentage is as high as

95% [6–8]. Currently, many of the world's water sources have been identified as polluted. A four-seasonal sampling (2003–2004) established the presence of various medications in the New York City watershed [9]. The plasma of sharks living in Florida's Caloosahatchee River contained detectable levels of six reuptake inhibitors, including the antidepressants citalopram, fluoxetine, fluvoxamine, paroxetine, sertraline and venlafaxine; in the same area, triclosan, a household disinfectant ingredient, was found at a significantly measurable level in dolphin blood plasma [10,11]. Researchers in Spain found painkillers, fever reducers, inflammatory agents, antibiotics, antilipemics and blockers in Madrid's river [12].

Antibiotics in water boost the immunity of microbes and lead to the emergence of novel pathogens [13]. The fluoroquinolone antibiotic ciprofloxacin (CPXN) is its family's most commonly used antibiotic [14,15]. The structural conformation of CPXN accounts for its high solubility in water (30 g L^{-1}) and contributes to its widespread presence in aquatic environments [16,17]. In effluent treatment facilities near Hyderabad, India, CPXN was found at concentrations higher than the highest therapeutic human plasma level [18]. Concentrations of up to 155.0 µg/L CPXN were found in a university hospital effluent in Brazil [19]. CPXN remains untreated in several hospital effluents in Germany and has been reported at wastewater treatment plants and natural water resources [20–22]. Sedimentation, filtration, disinfection, sludge treatment, oxidation, coagulation–precipitation, reverse osmosis and ion exchange are all used to remove pollutants [23–25]. The high price tag and the need for constant monitoring are two of the most significant drawbacks of these technologies. Nevertheless, the presence of pharmaceutical components in tap water proves that such techniques are not good enough to satisfy criteria for water safety [26–29]. Heterogeneous cracking involving light-absorbing-catalysts in contact with the reactants is one of the methodologies that has benefited from nanoscience. Although photocatalytic degradation has succeeded in degrading various hazardous organic pollutants and has provided advantages over classical approaches, its drawbacks include energy consumption and the production of harmful radicals [30]. Conversely, adsorption consumes less energy, is simple, has high efficiency, is easily implemented and doesn't liberate toxic compounds; its physical characteristics involve Van der Waals forces while its chemical ones include chemical bonding between pollutants and sorbents. Carbon has traditionally been employed to remove undesirable organic compounds and used in environmental applications as a sorbent and catalyst-supporting substrate. Carbon nanoparticles (CNPs) have been used to remove organic and inorganic contaminants; they first drew attention due to their large surface area, functional ability, remarkable adsorption capacities, ease of regeneration and resilience to corrosive media [31]. Given that the annual production of biowaste reaches 20 billion pounds distributed over about 70 countries [32], turning massive biowaste into valuable materials by fabricating carbonaceous materials (CRMs) from coffee waste would be of great interest.

This study planned to utilize coffee skin waste in formulating CRMs via pyrolysis in an oxygen-poor environment. The produced CRMs would be demineralized via boiling with an acid then downsized via milling to fabricate nanoparticles (CCNPs). The synthesized CCNPs would be characterized experimentally by physical means. Thereafter, CCNPs would be tested as sorbents for remediating water contaminated by pharmaceutical contaminants. The study includes investigating the impact of solution parameters on the performance of CCNPs in removing CPXN from water. In addition, the adsorption kinetics, isotherms and thermodynamics will be investigated.

2. Experimental Methodology

2.1. Materials

Hydrochloric acid (37% HCl) was provided by Sharlau, Madrid, Spain. Coffee skin waste (CSW) was acquired from a local market (KSA). CPXN-HCl powder was provided by Rhanboxy, Mumbai, India.

2.2. Fabrication of CCNPs

About 20.0 g CSWs were placed in a boat crucible, transferred into a tubular furnace, and carbonized at 600 °C for 2.0 h under a nitrogen stream (50 mL min^{-1}). About 5.0 g of carbon was placed in the stainless steel crucible of a vertical planetary ball mill (Netzspannungswashi, Germany) operated at 500 RPM for 10.0 h. The product was boiled with 100 mL of HCl (2.0 M) for 1.0 h. The CCNPs were dispersed in 200 mL of DW and sonicated for 10 min, filtered, rinsed with distilled water to about pH 6.5 and dried at 110 °C for 3.0 h.

2.3. Characterization of the CCNPs

The nanoparticles' phase purity was analyzed using a powder X-ray diffractometer (XRD) (Bruker, D8 Advance; Billerica, Miami, FL, USA). The superficial and detailed morphologies of CCNPs were investigated using scanning electron-energy dispersive microscopy (SEM-EDX) (JSM-IT300, Jeol, Tokyo, Japan). In addition, the functional groups on the surface of the CCNPs were analyzed by Fourier transform infrared spectroscopy (FTIR) with a KBr disk (Bruker TENSOR-FTIR, Miami, FL, USA). Also, the surface characteristics were analyzed via a ASAP 2020 Micromeritics surface analyzer, Miami, FL, USA.

2.4. Adsorption of CPXN on CCNPs

An experimental batch protocol was utilized to test the CPXN adsorption on the fabricated CCNPs in water. A 120 mL aqueous solution of 50 mg L^{-1} CPXN was combined with CCNPs and stirred. In order to examine the effects of both concentration and temperature, the adsorption process was also run with CPXN concentrations ranging from 10 to 50 mg L^{-1} within a temperature range of 20 to 50 °C. Additionally, the effect of pH was investigated by varying the pH of the pollutant solution from 2 to 11. The absorbance of CPXN was measured with a UV-Vis spectrophotometer (Shimadzu-2600i, Kyoto, Japan) at 273 nm, and Equation (1) was utilized to determine the pollutant adsorption capacity of the CCNPs (q_t, mg g^{-1}).

$$q_t = \frac{(C_o - C_t)V}{M} \quad (1)$$

C_o and C_t (mg L^{-1}) are the CPXN concentrations at the initial time and at t min.
V and M are the solution volume (mL) and the adsorbent mass (g).

The kinetics of CPXN adsorption onto the CCNPs was studied. The pseudo-first-order models (PFM) and pseudo-second-order models (PSM) expressed in Equations (2) and (3) were used to investigate the adsorption rate order. Furthermore, the step controlling adsorption was analyzed using the liquid film diffusion model (LFM) (Equation (4)) and the intraparticle diffusion model (IPM) (Equation (5)) [33].

$$\ln(q_e - q_t) = \ln q_e - k_1 \times t \quad (2)$$

$$\frac{1}{q_t} = \frac{1}{k_2 \times q_e^2 t} + \frac{1}{q_e} \quad (3)$$

$$q_t = K_{IP} \times t^{\frac{1}{2}} + C_i \quad (4)$$

$$\ln(1 - F) = -K_{LF} \times t \quad (5)$$

where: q_e (mg g^{-1}) is q_t at equilibrium; k_1 (min^{-1}): PFM factor; and k_2 (g mg^{-1} min^{-1}) PSM factor (which have been calculated from the slope and intercept values, respectively). K_{IP} (mg g^{-1} $min^{-0.5}$) and K_{LF} (min^{-1}) are the LFM and IPM constants (computed from their slope values). C_i (mg g^{-1}) is a boundary layer thickness factor [32].

As they are the most used isotherm representations, the Langmuir model (LM, Equation (6)) and the Freundlich model (FM, Equation (7)) were employed in investigating the monolayer and multilayer adsorption, respectively.

$$\frac{1}{q_e} = \frac{1}{K_L q_m} \times \frac{1}{C_e} + \frac{1}{K_L} \quad (6)$$

$$\ln q_e = \ln K_F + \frac{1}{n} \ln C_e \quad (7)$$

C_e (mg L^{-1}) is CPXN's concentration at equilibrium; K_L (L mg^{-1}) is the LIM constant, and K_F (L mg^{-1}) is that of FIM; q_m (mg g^{-1}) is the predicted maximum q_t and n is the Freundlich heterogeneity factor.

Thermodynamic studies were performed on CPXN adsorption by the engineered CCNPs. In order to determine the equilibrium constant Kc, the adsorbed and residual concentrations (C_{ad} and C_e, mg L^{-1}) were employed. The enthalpy (ΔH°, kJ mol^{-1}) values were determined from plots of Equation (8). The intercepts from the linear plots were utilized in computing the entropy values (ΔS°, kJ mol^{-1}), by plugging in the values from Equation (8) into Equation (9), and in calculating the Gibbs free energy (ΔG°, (kJ mol^{-1})).

$$\ln K_c = \frac{\Delta H^\circ}{RT} + \frac{\Delta S^\circ}{R} \quad (8)$$

$$\Delta G^\circ = \Delta H^\circ - T\Delta S^\circ \quad (9)$$

3. Results and Discussion

3.1. Characterization of the Fabricated CCNPs

SEM analysis was used to investigate the surface morphology of the as-prepared CCNPs (Figure 1a,b). A 1,000,000 times magnification showed that the prepared CCNPs were sized from 35.6 to 41.6 nm and it revealed high uniformity in the fabricated CCNPs. EDX analysis was also employed to survey the CCNP's elemental composition (Figure 1c). The produced CCNPs were composed mainly of carbon and oxygen in addition to minor amounts of Na, K, Ca, Al and Zn, which may indicate that the demineralization with HCl (2.0 M) was not efficient enough.

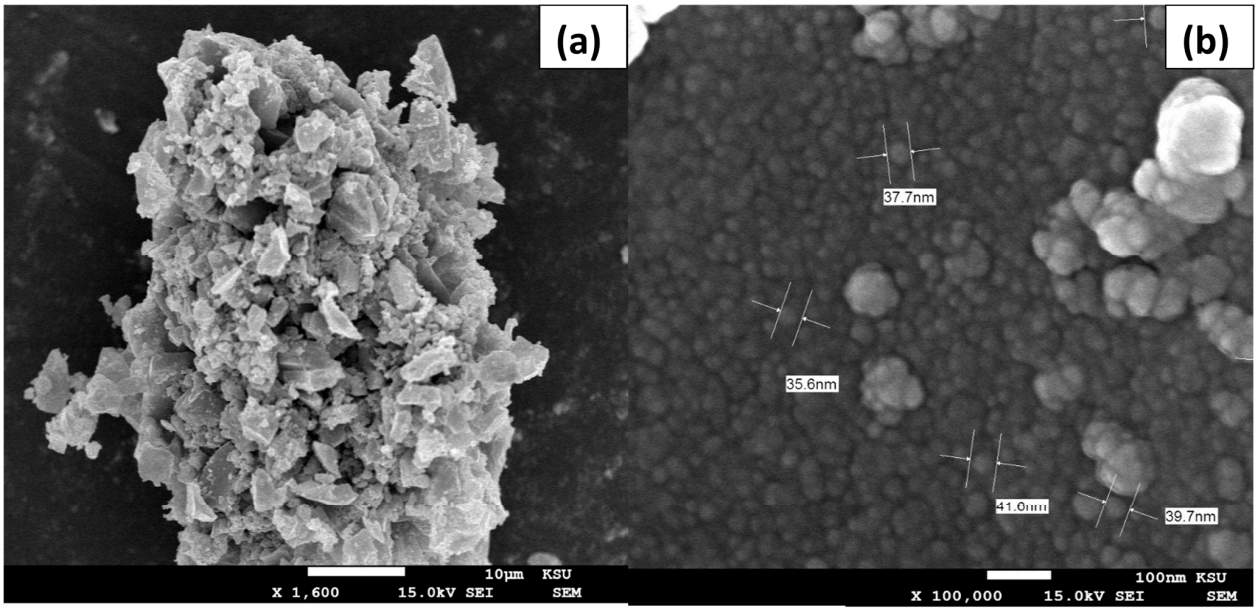

Figure 1. *Cont.*

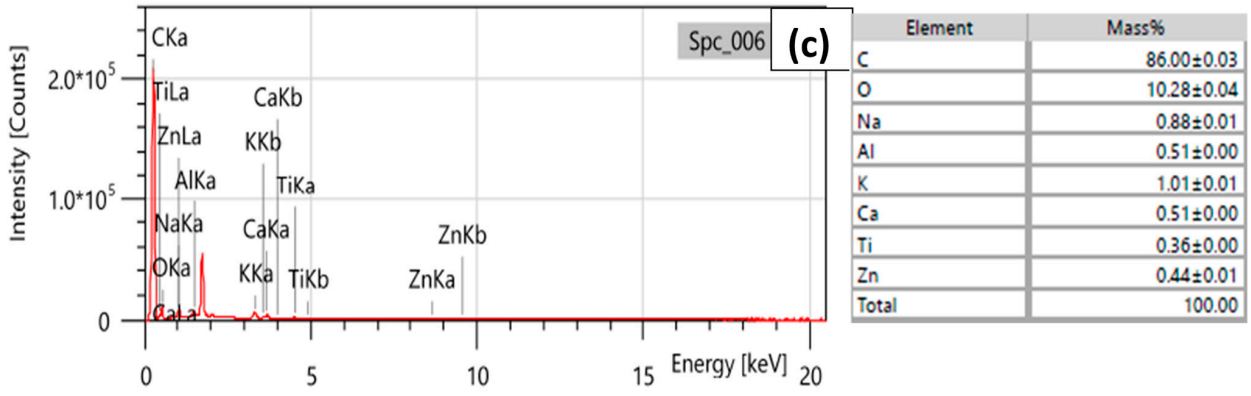

Figure 1. (**a**,**b**) SEM images; (**c**) EDX spectrum and elemental results of CCNPs fabricated via ball mill methodology.

XRD diffraction was employed to study the crystallinity and phase purity of the fabricated CCNPs. Figure 2a monitored the obtained diffraction pattern for the CCNPs; the peaks at 2θ° of 26.64 and 43.16 can be assigned to (002) and (100), the cubically constructed lattice of graphite (JCPDS No. 04-0850) [34,35]. The low intensity of these two bands indicated weakly crystallized CCNPs; this result can be supported by the minor tip around 2θ° of 10 corresponding to amorphous CCNPs. Additionally, because the CCNPs were fabricated from natural agricultural waste, it was expected that the trace amounts of Zn and Al revealed via the EDX analysis may explain the complexity of the obtained XRD pattern.

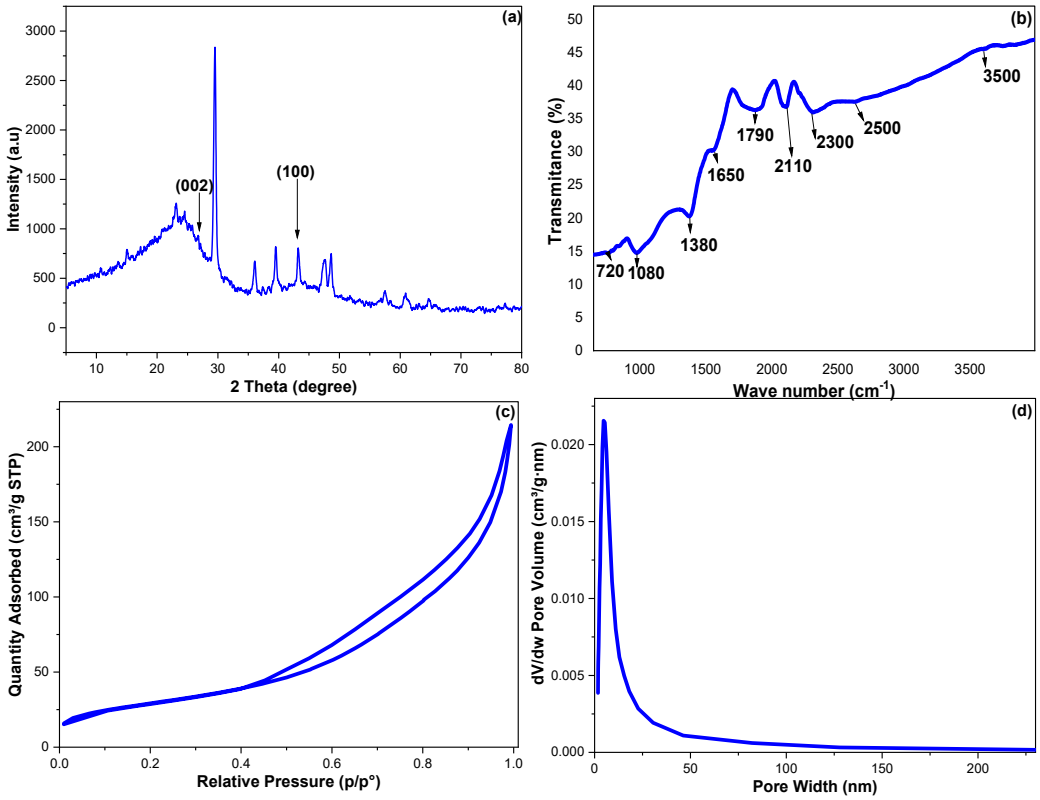

Figure 2. The obtained CCNP results of (**a**) XRD, (**b**) FTIR, (**c**) nitrogen adsorption–desorption isotherm and (**d**) pore size distribution.

Furthermore, the CCNP functional groups were examined utilizing FTIR (Figure 2b). The 750 and 1380 cm^{-1} peaks can be allocated to C-H in-plane wagging and C-H out-of-plane twisting vibrations. The bands at 1080 and 1790 cm^{-1} may be assigned to C-O and

C=O bonds, while the 2500 to 3500 cm^{-1} broadband belongs to the O-H stretching with an intermolecular hydrogen bonding. The 1650 and 2110 cm^{-1} were set to C=C stretching and the accumulated C=C, while the 2200 cm^{-1} peak can be attributed to C≡C stretching vibrations of terminal carbon atoms [34].

The CCNPs' surface features were investigated via the N_2 adsorption–desorption methodology, and Figure 2c,d monitored the resulting isotherm and pore distribution. The CCNPs' surface area (SA) was estimated utilizing the Brunauer–Emmett–Teller's (BET) relation, while the Barrett–Joyner–Halenda (BJH) calculation was employed to estimate the CCNPs' pore diameter and pore volume (PD and PV) [36]. The N_2 adsorption–desorption showed an ascending pattern with a desorption branch spread below a relative pressure value of 0.45. The fabricated CCNPs possessed a Type-H3-loop, distinctive for nonrigid-aggregated plate-like particles associated with cylindrical pores [37]. The CCNPs showed SA, PD and PV values of 105.638 m^2 g^{-1}, 19.38 Å and 0.301 cm^3 g^{-1}, respectively.

3.2. CPXN Adsorption onto CCNPs

Figure 3a depicts the contact time research of CPXN adsorption onto CCNPs. The adsorption of CPXN from water by the CCNPs reached equilibrium in 90 min with a q_t of 95.9 mg g^{-1}. In addition, the initial supplied concentration significantly impacts the adsorption process; Figure 3b shows direct proportionality between feed concentration and obtained qt, which reached 142.6 mg g^{-1} from the 100 mg L^{-1} CPXN. Increasing the initial concentration may produce an efficient force that aids in migrating CPXN toward the CCNPs' surface. Furthermore, the increase of q_t proportionally with feed concentrations revealed the capability of the CCNPs to remove high CPXN concentrations, and the inflation in Figure 3b showed the adequacy of a 5:12 adsorbent mass-to-solution volume ratio to treat up to 75 mg L^{-1} CPXN contamination. Conversely, raising the mixture's temperature was inversely related to the adsorbed amount of CPXN, as indicated by the drop of q_t to 114.3 and 79.2 mg g^{-1} from the 100 mg L^{-1} CPXN at 35 °C and 50 °C, respectively, which inferred exothermic adsorption. Due to its fast adsorption, short equilibrium time, comparatively high experimental q_t values, and low cost factor, this CCNP adsorbent is considered excellent compared to the existing carbonaceous adsorbents in the literature (Table 1).

The pH of the solution influences the availability and accessibility of functional groups on the CCNPs' surface and CPXN molecules [38]. The effect of changing the pH of the solution on the adsorption of pollutants was measured in terms of qt values at each pH value (Figure 3c). CPXN was better eliminated at pH 6.0, and its removal efficiency declined dramatically below pH 5.0 and above pH 8.0. At low pH, the readily accessible H+ may protonate the electron-rich sites on contaminants and/or CCNPs. On the other hand, -OH availability above pH 8.0 may compete with pollutants on adsorbent adsorption sites. The CPXN (pKa = 10.3) auxochrome group is protonated in water at low pH. These findings suggested that electrostatic attraction plays a considerable role in removing CPXN by CCNPs, consistent with the literature findings [39,40].

Table 1. Comparing the CCNPs with carbonaceous adsorbents in the literature in removing CPXN from water.

Adsorbent	Pollutant	Adsorption Capacity (mg g^{-1})	Reference
CCNPs	CPXN	142.6	This study
Activated commercial carbon	CPXN	13.6	[41]
FCNTs	CPXN	95.5	[42]
Carbon nanoparticles (CNPs)	CPXN	103.1	[34]
multiwall carbon nanotube (MWCNT)	CPXN	1.75	[43]
Magnetic carbon Fe_3O_4 composite	CPXN	90.1	[44]
Coal fly ash	CPXN	1.5	[44]
Elite	CPXN	33.1	[44]
Graphene oxide-polysulfone	CPXN	82.8	[45]
FCNTs-Fe_3O_4	CPXN	107.7	[46]

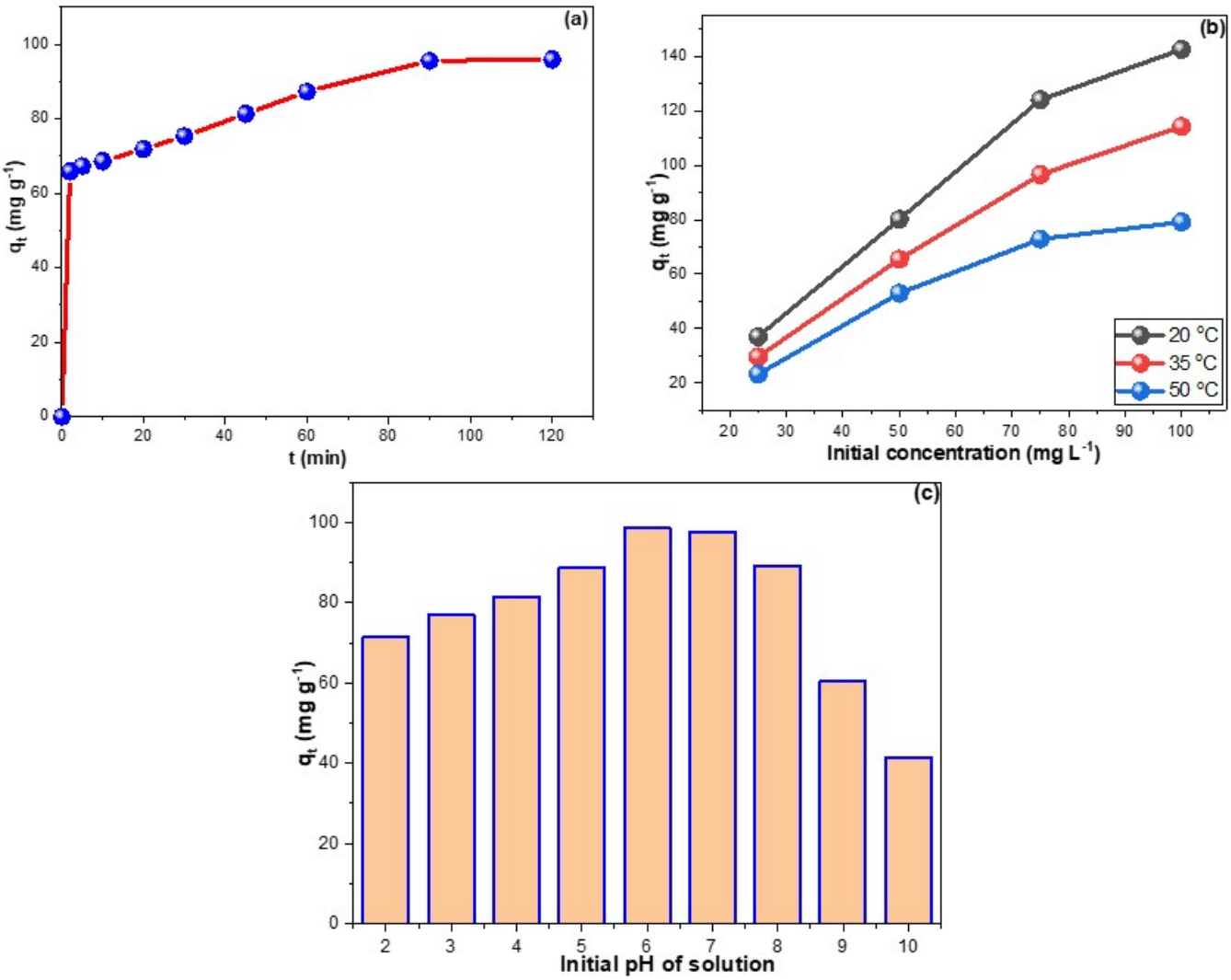

Figure 3. (**a**) time influence on CPXN adsorption by CCNPs; (**b**) effects of temperature and CPXN initial concentration on its removal by CCNPs and (**c**) the influence of initial solution pH on CPXN adsorption by the CCNPs.

3.3. Kinetics

Figure 4a,b illustrates the PFM and PSM regression lines of CPXN removal by CCNPs, and the results are in Table 2. The attained R^2 values prevailed in the agreement of CPXN adsorption to the PSM. LFM and IPM plots of CPXN removal by CCNPs were presented in Figure 4c,d; their outcomes were collected in Table 2. The CPXN adsorption on the CCNPs agreed with the LFM, which revealed the CPXN's excellent movement to the CCNPs' surface.

Table 2. Kinetics outcomes of CPXN adsorption onto CCNPs.

Adsorption Rate Order						
	PFM			PSM		
qe exp. (mg g^{-1})	qe cal. (mg g^{-1})	R^2	k_1 (min^{-1})	qe cal. (mg g^{-1})	R^2	k_2 (g mg^{-1} min^{-1})
95.936	18.250	0.858	0.049	87.298	0.969	0.005
Adsorption Mechanism						
	LFM			IPM		
K_{LF} (min^{-1})		R^2	K_{IP} (mg g^{-1} min$^{-0.5}$)	R^2		C
0.049		0.921	5.772	0.839		43.286

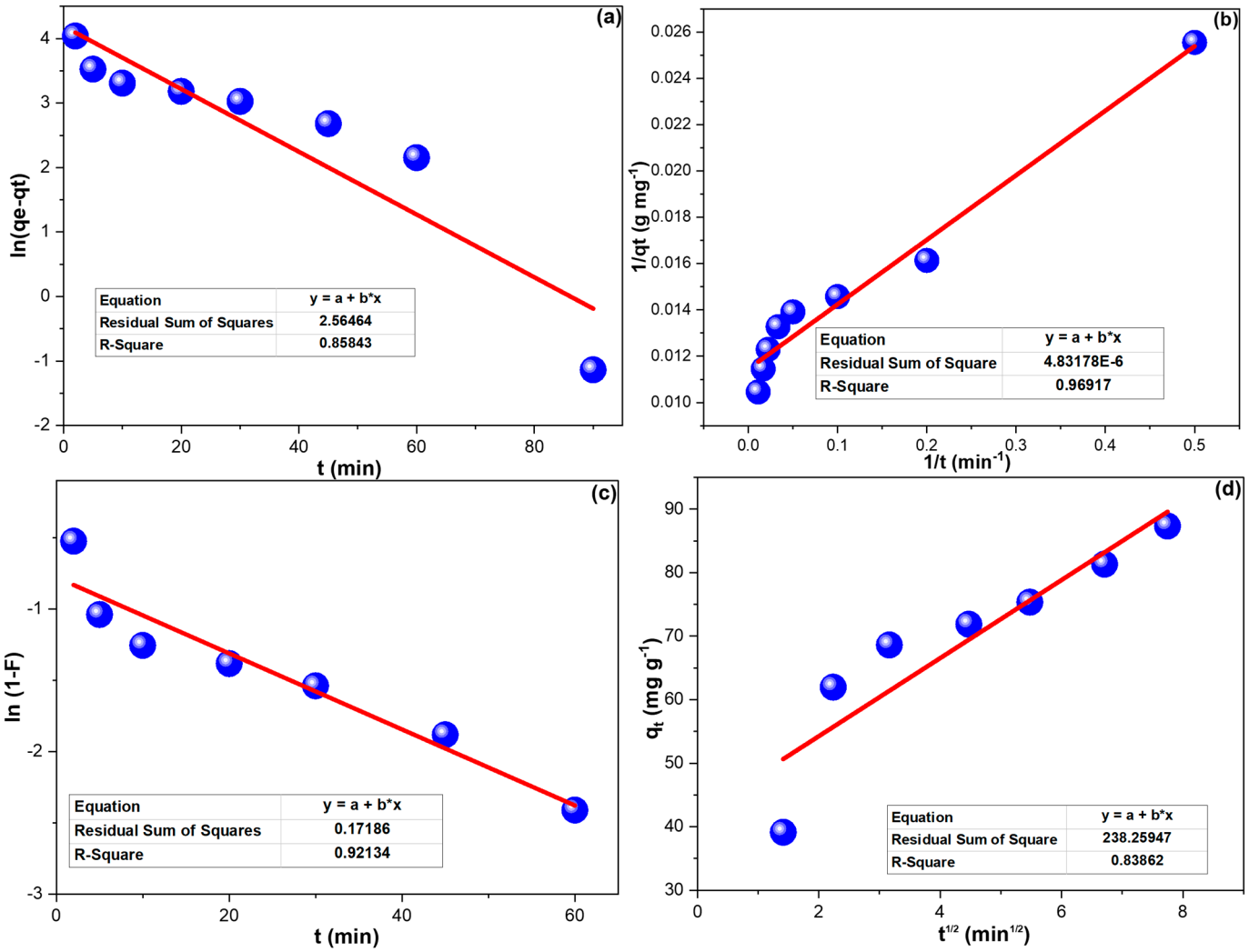

Figure 4. (**a**) PFM; (**b**) PSM; (**c**) LFM and (**d**) IPM investigations of CPXN adsorption onto CCNPs. (The * in the equation boxes refer to multiplication).

3.4. Isotherms and Thermodynamics

Figure 5 demonstrates the linear plots of FIM and FIM. The computed results for both isotherm models illustrated in Table 3 prevailed that CPXN adsorption onto CCNPs better fit the FIM model, and the 1/n of 0.126 implied favorable adsorption [47].

Table 3. The isotherms and thermodynamic obtaining of CPXN adsorption onto CCNPs within a 25 to 100 mg L^{-1} concentration range.

Isotherms						
Langmuir model			Freundlich model			
R^2 (a.u)	K_L (L mg^{-1})	q_m (mg g^{-1})	R^2 (a.u)	Kf (L mg^{-1})	1/n (a.u)	
0.848	2.020	89.653	0.927	58.252	0.126	
Thermodynamics						
Fed Conc. (mg L^{-1})	ΔH° (kJ mol^{-1})	ΔS° (kJ mol^{-1})	ΔG° (kJ mol^{-1}) 298 K	ΔG° (kJ mol^{-1}) 308 K	ΔG° (kJ mol^{-1}) 318 K	R^2 (a.u)
25	−46.859	−0.149	−2.552	−1.065	0.421	0.996
50	−25.811	−0.053	−10.047	−9.518	−8.989	1.000
75	−58.250	−0.192	−0.967	0.956	2.878	0.928
100	−43.737	−0.148	0.264	1.741	1.741	0.727

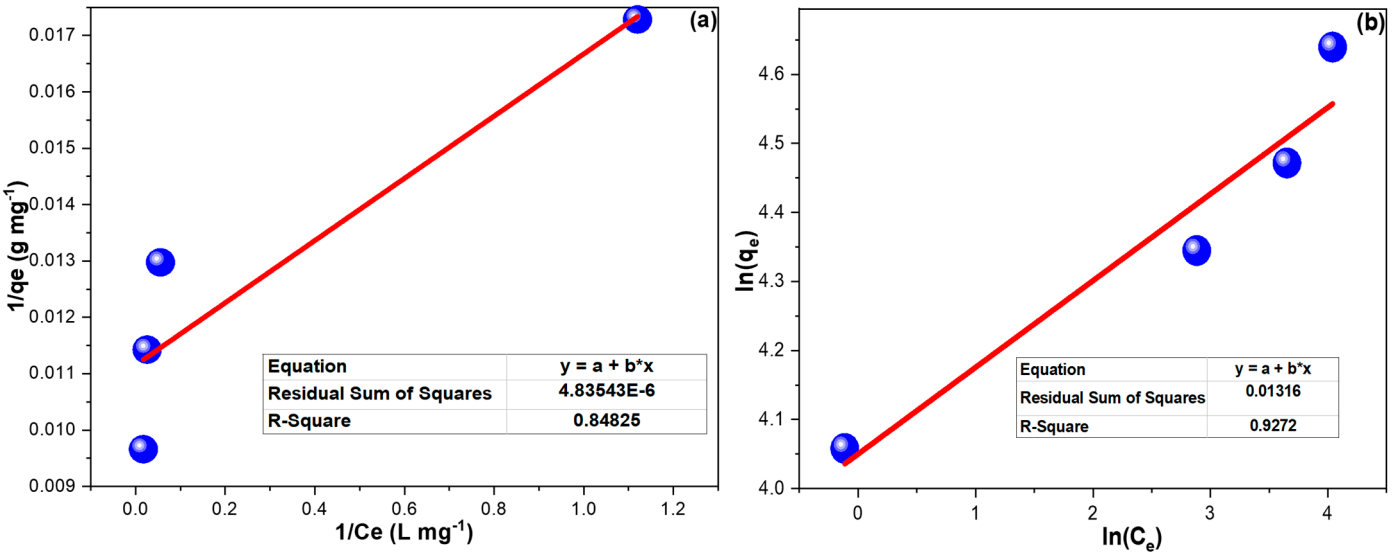

Figure 5. (**a**) LIM and (**b**) FIM investigations of CPXN adsorption onto CCNPs from 25, 50, 75 and 100 mg L^{-1} concentrations at 20 °C. (The * in the equation boxes refer to multiplication).

Figure 6a shows the linear plots of Equation (8) for CPXN concentrations of 25, 50, 75 and 100 mg L^{-1}.The obtained ΔH° values pointed to exothermic adsorption, and the resulting ΔG° suggested that CPXN adsorption occurred spontaneously [48]. Furthermore, the significant increase in the ΔG° at higher temperatures indicated that CPXN adsorption by CCNPs was temperature sensitive. The ΔG° values obtained with the four tested concentrations were less than 80.0 kJ mol^{-1}, indicating a physisorptive nature. Moreover, the negative ΔS° results supported the Freundlich outcome that the CPXN adsorption on the CCNPs was favorable [49].

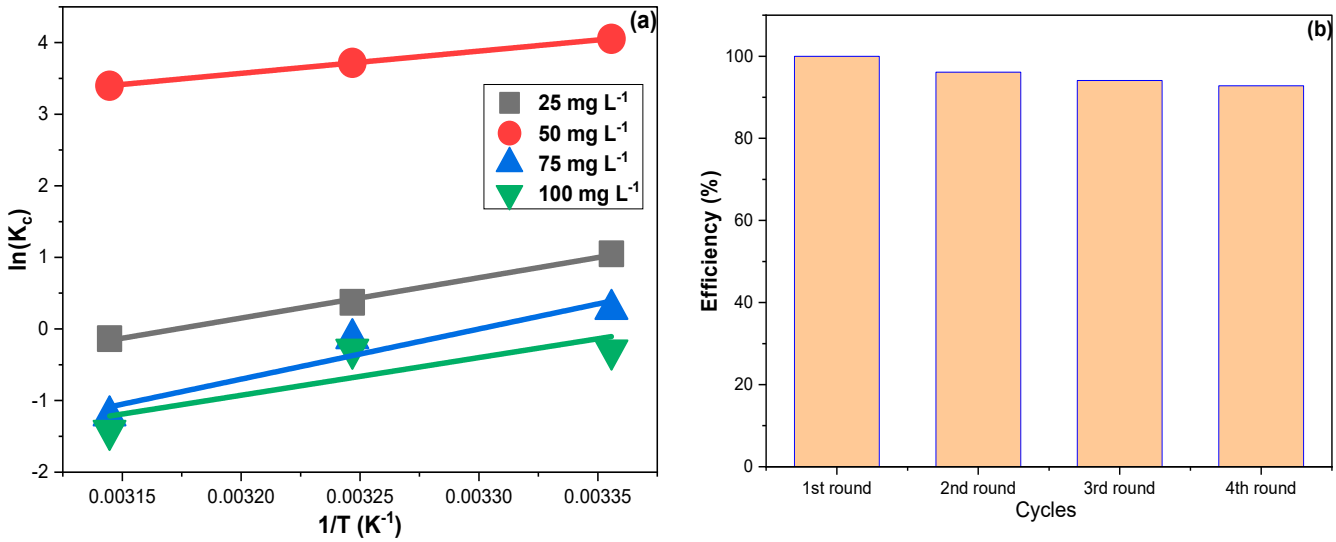

Figure 6. (**a**) The thermodynamic results for the adsorption of CPXN on the CCNPs within a temperature range of 20 °C to 50 °C using 25, 50, 75 and 100 mg L^{-1} CPXN solutions; (**b**) the CCNPs reuse in removing CPXN from aqueous solutions.

3.5. Reuse Study

It is crucial to investigate the adsorbent's reusability as an economic factor; hence the used CCNPs were regenerated via sonication with 20 mL of ethanol for 15 min and filtered; then, the sonication was duplicated with 20 mL, distilled, filtered, reactivated at 110 °C and employed for the next round. Figure 6b demonstrates the performance of CCNPs in

removing CPXN within four consecutive regeneration–reuse cycles. The CCNPs showed an RSD of 3.1%, average efficiency of 95.8% and least efficiency of 92.8%. The lowering of CCNP performance in the last cycles can be attributed to the adsorption agreement with LFM and FIM that implied the ease of CPXN penetration into the CCNP inner shells and the multilayer accumulation of CPXN on the CCNPs' surface. However, the CCNPs performed excellently throughout the four batches of contaminated water.

4. Conclusions

CCNPs were fabricated from coffee skin as cheap agricultural waste via carbonization in a tubular furnace under a nitrogen stream followed by a vertical planetary ball milling methodology. The SEM revealed CCNPs within the range of 35.6 to 41.6 nm. In the N_2 adsorption–desorption analysis, the CCNPs possessed SA, PD and PV values of 105.638 $m^2\ g^{-1}$, 19.38 Å and 0.301 $cm^3\ g^{-1}$, respectively. Thereafter, CCNPs were tested for removing CPXN and showed a q_t of 142.6 mg g^{-1} from the 100 mg L^{-1} solution. Raising the solution's temperature affected q_t inversely, as indicated by the drop of q_t to 114.3 and 79.2 mg g^{-1} from the 100 mg L^{-1} CPXN at 35 °C and 50 °C, compared to 142.6 mg g^{-1} at 20 °C, which indicated an exothermic adsorption. CPXN was better eliminated at pH 6.0, and its removal efficiency declined dramatically below pH 5.0 and above pH 8.0. Kinetically, CPXN adsorption fitted the PSM and agreed with the LFM, which indicated the CPXNs' preference for the CCNPs' surface. The obtained ΔH° values supported an exothermic nature, and the resulting ΔG° revealed the spontaneity of CPXN adsorption. Moreover, the negative ΔS° results supported the Freundlich outcome that the CPXN adsorption on the CCNPs was favorable. The CCNPs had an RSD of 3.1%, average efficiency of 95.8% and least efficiency of 92.8% in the four reuse cycles. The lowering of CCNP performance in the last cycles can be attributed to the adsorption agreement with LFM and FIM that implied the ease of CPXN penetration into the CCNP inner shells and the multilayered accumulation of CPXN on the CCNPs' surface. However, the CCNPs performed excellently throughout the four batches of contaminated water.

Author Contributions: Conceptualization, B.Y.A.; methodology, M.S.; formal analysis, M.A.; investigation, B.Y.A.; resources, M.S.; data curation, B.Y.A.; writing—original draft preparation M.S.; writing—review and editing, B.Y.A.; supervision, B.Y.A.; project administration, M.S.; funding acquisition, M.S. All authors have read and agreed to the published version of the manuscript.

Funding: The authors extend their appreciation to the Deanship of Scientific Research, Imam Mohammad Ibn Saud Islamic University (IMSIU), Saudi Arabia, for funding this research work through Grant No. (221419003).

Data Availability Statement: All reported results are available from the corresponding author under reasonable request.

Conflicts of Interest: The authors declare no conflict of interest and that the funders had no role in the study's design or in the collection, analyses or interpretation of data, in the writing of the manuscript or in the decision to publish the results.

References

1. Cabrera-Lafaurie, W.A.; Román, F.R.; Hernández-Maldonado, A.J. Transition metal modified and partially calcined inorganic–organic pillared clays for the adsorption of salicylic acid, clofibric acid, carbamazepine, and caffeine from water. *J. Colloid Interface Sci.* **2012**, *386*, 381–391. [CrossRef] [PubMed]
2. Yang, Y.; Ok, Y.S.; Kim, K.-H.; Kwon, E.E.; Tsang, Y.F. Occurrences and removal of pharmaceuticals and personal care products (PPCPs) in drinking water and water/sewage treatment plants: A review. *Sci. Total Environ.* **2017**, *596*, 303–320. [CrossRef] [PubMed]
3. Manahan, S. *Environmental Chemistry*; CRC Press: Leiden, The Netherlands, 2017.
4. Verma, J.; Pant, H.; Sign, S.; Tiwari, A. Marine pollution, sources, effect and management. In *Three Major Dimensions of Life: Environment, Agriculture and Health*; Society of Biological Sciences and Rural Development: Prayagraj, India, 2020; pp. 270–276.
5. Kurwadkar, S.; Kanel, S.R.; Nakarmi, A. Groundwater pollution: Occurrence, detection, and remediation of organic and inorganic pollutants. *Water Environ. Res.* **2020**, *92*, 1659–1668. [CrossRef] [PubMed]

6. Ruhoy, I.S.; Daughton, C.G. Beyond the medicine cabinet: An analysis of where and why medications accumulate. *Environ. Int.* **2008**, *34*, 1157–1169. [CrossRef] [PubMed]
7. Zhao, Y.; Xiao, X. Environmental Antibiotics: Exposure Monitoring and Health Endpoints. In *Emerging Chemicals and Human Health*; Springer: Singapore, 2019; pp. 165–178.
8. Gupta, R.; Sati, B.; Gupta, A. Treatment and recycling of wastewater from pharmaceutical industry. In *Advances in Biological Treatment of Industrial Waste Water and Their Recycling for a Sustainable Future*; Springer: Singapore, 2019; pp. 267–302.
9. Palmer, P.M.; Wilson, L.R.; O'Keefe, P.; Sheridan, R.; King, T.; Chen, C.Y. Sources of pharmaceutical pollution in the New York City Watershed. *Sci. Total Environ.* **2008**, *394*, 90–102. [CrossRef]
10. Deo, R.P. Pharmaceuticals in the surface water of the USA: A review. *Curr. Environ. Health Rep.* **2014**, *1*, 113–122. [CrossRef]
11. Fair, P.A.; Lee, H.-B.; Adams, J.; Darling, C.; Pacepavicius, G.; Alaee, M.; Bossart, G.D.; Henry, N.; Muir, D. Occurrence of triclosan in plasma of wild Atlantic bottlenose dolphins (Tursiops truncatus) and in their environment. *Environ. Pollut.* **2009**, *157*, 2248–2254. [CrossRef]
12. Alonso, S.G.; Catalá, M.; Maroto, R.R.; Gil, J.L.R.; de Miguel, Á.G.; Valcárcel, Y. Pollution by psychoactive pharmaceuticals in the Rivers of Madrid metropolitan area (Spain). *Environ. Int.* **2010**, *36*, 195–201. [CrossRef]
13. Fu, J.; Lee, W.-N.; Coleman, C.; Nowack, K.; Carter, J.; Huang, C.-H. Removal of pharmaceuticals and personal care products by two-stage biofiltration for drinking water treatment. *Sci. Total Environ.* **2019**, *664*, 240–248. [CrossRef]
14. Veclani, D.; Melchior, A. Adsorption of ciprofloxacin on carbon nanotubes: Insights from molecular dynamics simulations. *J. Mol. Liq.* **2020**, *298*, 111977. [CrossRef]
15. Rusu, A.; Hancu, G.; Uivaroşi, V. Fluoroquinolone pollution of food, water and soil, and bacterial resistance. *Environ. Chem. Lett.* **2015**, *13*, 21–36. [CrossRef]
16. Roca Jalil, M.E.; Baschini, M.; Sapag, K. Removal of ciprofloxacin from aqueous solutions using pillared clays. *Materials* **2017**, *10*, 1345. [CrossRef] [PubMed]
17. Varanda, F.; Pratas de Melo, M.J.; Caco, A.I.; Dohrn, R.; Makrydaki, F.A.; Voutsas, E.; Tassios, D.; Marrucho, I.M. Solubility of antibiotics in different solvents. 1. Hydrochloride forms of tetracycline, moxifloxacin, and ciprofloxacin. *Ind. Eng. Chem. Res.* **2006**, *45*, 6368–6374. [CrossRef]
18. Larsson, D.J.; de Pedro, C.; Paxeus, N. Effluent from drug manufactures contains extremely high levels of pharmaceuticals. *J. Hazard. Mater.* **2007**, *148*, 751–755. [CrossRef] [PubMed]
19. Martins, A.F.; Vasconcelos, T.G.; Henriques, D.M.; Frank, C.d.S.; König, A.; Kümmerer, K. Concentration of ciprofloxacin in Brazilian hospital effluent and preliminary risk assessment: A case study. *CLEAN–Soil Air Water* **2008**, *36*, 264–269. [CrossRef]
20. Magdaleno, A.; Juárez, Á.B.; Dragani, V.; Saenz, M.E.; Paz, M.; Moretton, J. Ecotoxicological and genotoxic evaluation of Buenos Aires city (Argentina) hospital wastewater. *J. Toxicol.* **2014**, 1–11. [CrossRef]
21. Östman, M.; Lindberg, R.H.; Fick, J.; Björn, E.; Tysklind, M. Screening of biocides, metals and antibiotics in Swedish sewage sludge and wastewater. *Water Res.* **2017**, *115*, 318–328. [CrossRef]
22. Azevedo, F.C.R.; Vaz, I.C.D.; Barbosa, F.A.R.; Magalhães, S.M. Toxicological effects of ciprofloxacin and chlorhexidine on growth and chlorophyll a synthesis of freshwater cyanobacteria. *Braz. J. Pharm. Sci.* **2019**, *55*, 1–11. [CrossRef]
23. Seo, P.W.; Bhadra, B.N.; Ahmed, I.; Khan, N.A.; Jhung, S.H. Adsorptive removal of pharmaceuticals and personal care products from water with functionalized metal-organic frameworks: Remarkable adsorbents with hydrogen-bonding abilities. *Sci. Rep.* **2016**, *6*, 34462. [CrossRef]
24. Lima, E.C. Removal of emerging contaminants from the environment by adsorption. *Ecotoxicol. Environ. Saf.* **2018**, *150*, 1–17.
25. Xu, Y.; Liu, T.; Zhang, Y.; Ge, F.; Steel, R.M.; Sun, L. Advances in technologies for pharmaceuticals and personal care products removal. *J. Mater. Chem. A* **2017**, *5*, 12001–12014. [CrossRef]
26. Adeleye, A.S.; Conway, J.R.; Garner, K.; Huang, Y.; Su, Y.; Keller, A.A. Engineered nanomaterials for water treatment and remediation: Costs, benefits, and applicability. *Chem. Eng. J.* **2016**, *286*, 640–662. [CrossRef]
27. Teh, C.Y.; Budiman, P.M.; Shak, K.P.Y.; Wu, T.Y. Recent advancement of coagulation–flocculation and its application in wastewater treatment. *Ind. Eng. Chem. Res.* **2016**, *55*, 4363–4389. [CrossRef]
28. Jiang, J.-Q. The role of coagulation in water treatment. *Curr. Opin. Chem. Eng.* **2015**, *8*, 36–44. [CrossRef]
29. Cui, H.; Huang, X.; Yu, Z.; Chen, P.; Cao, X. Application progress of enhanced coagulation in water treatment. *RSC Adv.* **2020**, *10*, 20231–20244. [CrossRef]
30. Stara, J.F.; Kello, D.; Durkin, P. Human health hazards associated with chemical contamination of aquatic environment. *Environ. Health Perspect.* **1980**, *34*, 145–158. [CrossRef]
31. Almufarij, R.S.; Abdulkhair, B.Y.; Salih, M.; Alhamdan, N.M. Sweep-Out of Tigecycline, Chlortetracycline, Oxytetracycline, and Doxycycline from Water by Carbon Nanoparticles Derived from Tissue Waste. *Nanomaterials* **2022**, *12*, 3617. [CrossRef]
32. Ibrahim, T.G.; Almufarij, R.S.; Abdulkhair, B.Y.; Ramadan, R.S.; Eltoum, M.S.; Abd Elaziz, M.E. A Thorough Examination of the Solution Conditions and the Use of Carbon Nanoparticles Made from Commercial Mesquite Charcoal as a Successful Sorbent for Water Remediation. *Nanomaterials* **2023**, *13*, 1485. [CrossRef]
33. Elamin, M.R.; Abdulkhair, B.Y.; Elzupir, A.O. Insight to aspirin sorption behavior on carbon nanotubes from aqueous solution: Thermodynamics, kinetics, influence of functionalization and solution parameters. *Sci. Rep.* **2019**, *9*, 12795. [CrossRef]

34. Almufarij, R.S.; Abdulkhair, B.Y.; Salih, M.; Aldosari, H.; Aldayel, N.W. Optimization, Nature, and Mechanism Investigations for the Adsorption of Ciprofloxacin and Malachite Green onto Carbon Nanoparticles Derived from Low-Cost Precursor via a Green Route. *Molecules* **2022**, *27*, 4577. [CrossRef]
35. Abdulkhair, B.Y.; Elamin, M.R. Low-Cost Carbon Nanoparticles for Removing Hazardous Organic Pollutants from Water: Complete Remediation Study and Multi-Use Investigation. *Inorganics* **2022**, *10*, 136. [CrossRef]
36. Brunauer, S.; Emmett, P.H.; Teller, E. Adsorption of gases in multimolecular layers. *J. Am. Chem. Soc.* **1938**, *60*, 309–319. [CrossRef]
37. Thommes, M.; Kaneko, K.; Neimark, A.V.; Olivier, J.P.; Rodriguez-Reinoso, F.; Rouquerol, J.; Sing, K.S. Physisorption of gases, with special reference to the evaluation of surface area and pore size distribution (IUPAC Technical Report). *Pure Appl. Chem.* **2015**, *87*, 1051–1069. [CrossRef]
38. Ayodele, O.; Olusegun, S.J.; Oluwasina, O.O.; Okoronkwo, E.A.; Olanipekun, E.O.; Mohallem, N.D.; Guimarães, W.G.; Gomes, B.L.d.M.; Souza, G.d.O.; Duarte, H.A. Experimental and theoretical studies of the adsorption of Cu and Ni ions from wastewater by hydroxyapatite derived from eggshells. *Environ. Nanotechnol. Monit. Manag.* **2021**, *15*, 100439. [CrossRef]
39. Elamin, M.R.; Ibnaouf, K.H.; Elamin, N.Y.; Adam, F.A.; Alolayan, A.H.; Abdulkhair, B.Y. Spontaneous Adsorption and Efficient Photodegradation of Indigo Carmine under Visible Light by Bismuth Oxyiodide Nanoparticles Fabricated Entirely at Room Temperature. *Inorganics* **2022**, *10*, 65. [CrossRef]
40. Tsai, C.-Y.; Lin, P.-Y.; Hsieh, S.-L.; Kirankumar, R.; Patel, A.K.; Singhania, R.-R.; Dong, C.-D.; Chen, C.-W.; Hsieh, S. Engineered mesoporous biochar derived from rice husk for efficient removal of malachite green from wastewaters. *Bioresour. Technol.* **2022**, *347*, 126749. [CrossRef]
41. Peñafiel, M.E.; Matesanz, J.M.; Vanegas, E.; Bermejo, D.; Mosteo, R.; Ormad, M.P. Comparative adsorption of ciprofloxacin on sugarcane bagasse from Ecuador and on commercial powdered activated carbon. *Sci. Total Environ.* **2021**, *750*, 141498. [CrossRef]
42. Elamin, M.R.; Abdulkhair, B.Y.; Elzupir, A.O. Removal of ciprofloxacin and indigo carmine from water by carbon nanotubes fabricated from a low-cost precursor: Solution parameters and recyclability. *Ain Shams Eng. J.* **2023**, *14*, 101844. [CrossRef]
43. Avcı, A.; İnci, İ.; Baylan, N. Adsorption of ciprofloxacin hydrochloride on multiwall carbon nanotube. *J. Mol. Struct.* **2020**, *1206*, 127711. [CrossRef]
44. Mao, H.; Wang, S.; Lin, J.-Y.; Wang, Z.; Ren, J. Modification of a magnetic carbon composite for ciprofloxacin adsorption. *J. Environ. Sci.* **2016**, *49*, 179–188. [CrossRef]
45. Indherjith, S.; Karthikeyan, S.; Monica, J.H.R.; Krishna Kumar, K. Technology. Graphene oxide & reduced graphene oxide polysulfone nanocomposite pellets: An alternative adsorbent of antibiotic pollutant-ciprofloxacin. *Sep. Sci. Technol.* **2019**, *54*, 667–674.
46. Yousefi, M.; Gholami, M.; Oskoei, V.; Mohammadi, A.A.; Baziar, M.; Esrafili, A. Comparison of LSSVM and RSM in simulating the removal of ciprofloxacin from aqueous solutions using magnetization of functionalized multi-walled carbon nanotubes: Process optimization using GA and RSM techniques. *J. Environ. Chem. Eng.* **2021**, *9*, 105677. [CrossRef]
47. Alrobei, H.; Prashanth, M.; Manjunatha, C.; Kumar, C.P.; Chitrabanu, C.; Shivaramu, P.D.; Kumar, K.Y.; Raghu, M. Adsorption of anionic dye on eco-friendly synthesised reduced graphene oxide anchored with lanthanum aluminate: Isotherms, kinetics and statistical error analysis. *Ceram. Int.* **2021**, *47*, 10322–10331. [CrossRef]
48. Elamin, M.R.; Abdulkhair, B.Y.; Algethami, F.K.; Khezami, L. Linear and nonlinear investigations for the adsorption of paracetamol and metformin from water on acid-treated clay. *Sci. Rep.* **2021**, *11*, 13606. [CrossRef] [PubMed]
49. Ncibi, M.C.; Sillanpää, M. Optimizing the removal of pharmaceutical drugs Carbamazepine and Dorzolamide from aqueous solutions using mesoporous activated carbons and multi-walled carbon nanotubes. *J. Mol. Liq.* **2017**, *238*, 379–388. [CrossRef]